JOURNAL OF SOLID STATE CHEMISTRY 113, 163–167 (1994)

DTG Curves of Selective Oxidation of Submicrometer Mixed Valency Spinels: Data Table for the Oxidation Temperature of Transition Metals and Its Relation to the Cation–Oxygen Distance

B. Gillot

Laboratoire de Recherche sur la Réactivité des Solides, URA 23 Faculté des Sciences Mirande, B.P. 138, 21004 Dijon Cedex, France

Received November 1, 1993; in revised form February 4, 1994; accepted February 9, 1994

Over the temperature range 150–550°C, the temperatures of oxidation peaks of transition metal ions in submicrometer-sized ferrites with the spinel structure, obtained by DTG, have been related to their cation–oxygen distances. A data table comparing oxidation temperature and cation–oxygen distance in both octahedral and tetrahedral sites for some oxidizable cations has been established. © 1994 Academic Press, Inc.

INTRODUCTION

The distribution, valence states, and oxidation temperatures of transition metal ions in oxospinels have long been of interest, both because of their structural, magnetic, and electrical properties and because of their technological usefulness. Concerning the submicrometer spinel oxides containing oxidizable ions such as Cu^{+}, Fe^{2+}, Mn^{2+}, Mn^{3+}, Mo^{3+}, and V^{3+} we have used a quantitative analysis by DTG (1) to obtain a direct measure of the mixed-valent distribution over both tetrahedral *A* and octahedral *B* sites, even where a given atom, such as iron or manganese, may have the $M^{(n+1)+}/M^{n+}$ redox couple for *A* sites overlapping the $M^{(n+1)+}/M^{n+}$ redox couple for *B* sites.

We have shown that these finely divided spinel powders (crystallite size below 100 nm) prepared at low temperatures can be oxidized at either *A* or *B* sites in cation-deficient spinels at specific temperatures characteristic of each oxidizable cation. What governs the temperature at which oxidation occurs is the activation energy for the ion jump and not that for electron transfer (2). For example, the *B*-site Fe^{2+} ions are more mobile than the *A*-site Fe^{2+} ions, so that they are oxidized near 200°C, whereas the *A* sites are only oxidized above 400°C. Such a difference of reactivity is evidence of a more covalent character of the tetrahedral Fe–O bond (3).

The aim of the present paper was to give some examples drawn from those substituted ferrites where the oxidation temperature might be closely associated with the nature, charge, and position of cations in the tetrahedral and octahedral sites of the spinel lattice. For this purpose, the effect of crystallite size and oxygen pressure on the oxidation temperature have also been considered.

EXPERIMENTAL

Simple oxalic salts $(Fe_{1-x-y}M_xM_y)C_2O_4 \cdot 2H_2O$ or complex oxalic salts $(NH_4)_3[Fe_{1-x-y}M_xM_y(C_2O_4)_3] \cdot 3H_2O$, as well as coprecipitates of hydroxydes, were used to combine iron with other elements, in particular chromium, manganese, copper, molybdenum, and titanum. These precursors, decomposed either in air or preferably in a controlled atmosphere, lead to highly divided oxides exhibiting specific areas of several hundred square meters per gram. Considering their very high state of division, these phases exhibit exceptional reactivity, in particular with redox media such as H_2–H_2O–N_2 gas mixtures. Treated under these conditions between 300 and 400°C, they will undergo a controlled reduction that will bring them to the state of submicrometer mixed valency spinels which have a crystallite size of the order of a few tens of nanometers (40–60 nm) (4).

Thus it becomes possible to oxidize not only Fe^{2+} ions below 600°C but, what is more original yet, ions such as Mn^{2+}, Mo^{3+}, Cu^{+}, and V^{3+}, while retaining the spinel lattice to generate nonstoichiometric phases by cation vacancies. The general formula can be expressed in the form $Fe_{3-x}M_xO_{4+\delta}$ (M = Mn, Mo, Cu, ...) with $\delta = 0.5$ for one exchanged electron, $\delta = 1$ for two exchanged electrons, $\delta = 1.5$ for three exchanged electrons, etc. (5).

These finely divided spinels exhibit a quite specific reactivity with oxygen that is characterized by the appearance of a series of oxidation phenomena at relatively low temperatures. Using thermogravimetry under very strict and well defined experimental conditions and using sample quantities of the order of 4 to 6 mg well sprayed in the sample holder, we have been able to show that the peaks observed by DTG were proportional to the content in oxidized Fe^{2+}, Mn^{2+}, Mo^{3+}, Cu^{+}, and V^{3+} ions.

0022-4596/94 $6.00

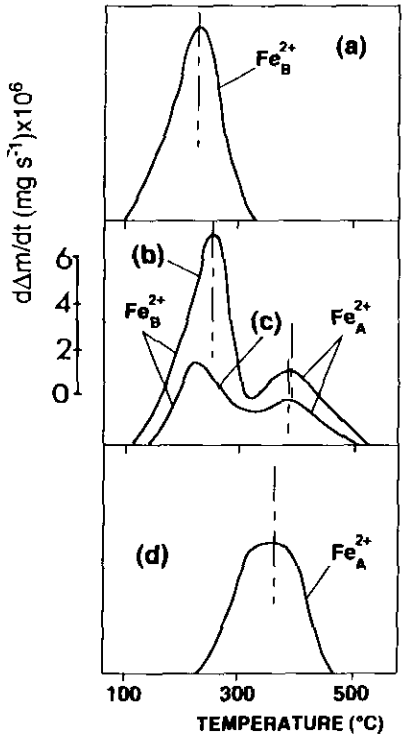

FIG. 1. DTG curves $d\Delta m/dt = f(T)$ for (a) Fe_3O_4; (b) $Fe_{3-x}Ti_xO_4$ with $x = 0.82$; (c) $Fe_{3-x}Cr_xO_4$ with $x = 0.80$; (d) $FeCr_2O_4$.

DETERMINATION OF THE OXIDATION PEAK TEMPERATURE FOR OXIDIZABLE CATIONS IN A SPINEL STRUCTURE

By reference to spinels having only iron as the oxidizable cation and in which its distribution is well known, such as Fe_3O_4 with Fe^{2+} ions at *B* sites and $FeCr_2O_4$ with Fe^{2+} ions at *A* sites, which present an oxidation process in one stage (Fig. 1, curves a and d), we also report in this figure the DTG curves for a Ti- and a Cr-substituted magnetite with Fe^{2+} ions in each site (curves b and c). In both cases, the oxidation in the cation-deficient spinel takes place in two stages (6), each revealing a first peak near 200°C and a second peak near 400°C due to the oxidation of Fe^{2+} ions of *B* sites and *A* sites, respectively. When cations other than iron are in a situation where they might oxidize, as with manganese (7, 8), molybdenum (9), copper (10), or vanadium (11), the oxidation behavior is more complex, as shown in Fig. 2, where five or three separate peaks within the range 200–530°C can be observed after desummation. Thus, it has been possible not only to determine complex distributions from a quantitative analysis of different oxidizable cations in each site (1, 12) but also to evaluate an oxidation temperature which is characteristic of each cation.

However, as the peaks exhibit a tendency to overlap, the desummation has been confirmed by selective oxidation and modeling. Figure 3 shows the profile of the peak attributed to Mo^{3+} ions after selective oxidation under isothermal conditions (155°C for 24 hr) of Fe^{2+} ions of *B* sites (curves a, b, and c). Therefore, the ascending branch corresponding to the curve c represents only the oxidation of Mo^{3+} ions. A similar experimental procedure was adopted for the oxidation of Mo^{4+} ions on *B* sites after elimination by selective oxidation of Fe^{2+} and Mo^{3+} ions (330°C for 24 hr). Curves d, e, and f show the different stages of progressive disappearance of the peak resulting of the Mo^{3+} ion oxidation.

Moreover, the possibility of oxidizing the different cations independently under isothermal conditions and of determining the kinetic parameters can provide interesting data for a modeling of the DTG curves. As in the case of the oxidation of submicrometer spinel ferrites in cation-deficient spinels, the reaction kinetics is acceptably interpreted by a law of diffusion of vacancies generated at the solid–gas interface; the only kinetic parameter of the reaction is the chemical diffusion coefficient. The model of a chemical diffusion coefficient with three parameters (frequency factor, thermal excited energy, and excited volume) permits one to explain the experiment curves which are obtained under isothermal and nonisothermal conditions. Thus, the DTG peaks corresponding to the

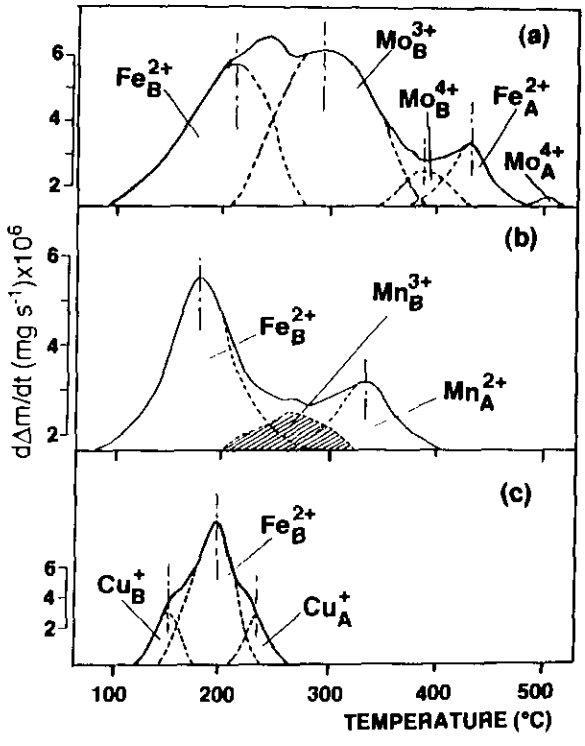

FIG. 2. DTG curves $d\Delta m/dt = f(T)$ (—) and desummation of spectra (---) of oxidation process for spinels with two oxidizable cations. (a) $Fe_{3-x}Mo_xO_4$ with $x = 0.58$; (b) $Fe_{3-x}Mn_xO_4$ with $x = 0.05$; (c) $Fe_{3-x}Cu_xO_4$ with $x = 0.32$.

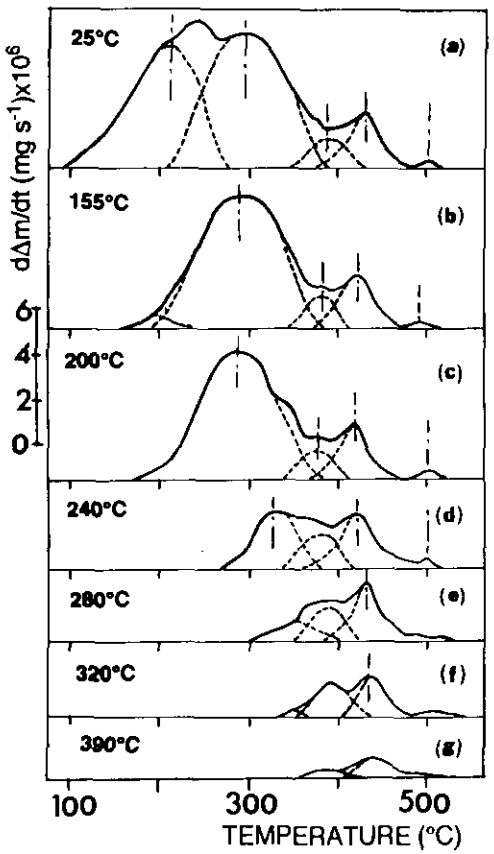

FIG. 3. DTG curves $d\Delta m/dt = f(T)$ for $Fe_{3-x}Mo_xO_4$ with $x = 0.58$ showing the disappearance of the first (Fe^{2+} ions, curves a and b) and second peak (Mo^{3+} ions, curves d and e) after selective oxidation. The indicated temperatures correspond to a selective isothermal oxidation for 24 hr.

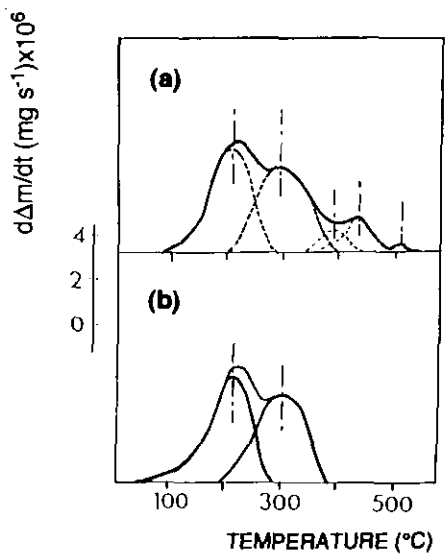

FIG. 4. DTG curves $d\Delta m/dt = f(T)$ (—) and desummation of spectra (---) for $Fe_{3-x}Mo_xO_4$. (a) Experimental curve and (b) modeled curve for Fe^{2+} and Mo^{3+} oxidations.

oxidation of Fe^{2+} and Mo^{3+} ions have been recalculated with the help of a computer (12). In Fig. 4, we can see that the profile of the experimental DTG peaks corresponding to Fe^{2+} and Mo^{3+} ions obtained after desummation (curve a) is comparable to the DTG peaks calculated from the isothermal kinetic parameter (curve b). This is consistent with the possibility of differentiating the oxidation peaks from DTG curves and leads to the existence of a definite oxidation temperature for each oxidizable cation. However, these oxidation temperatures are only valid for the same particle size and for oxidation in air.

The influence of crystallite size on the oxidation temperature for the same composition and oxygen pressure is shown in Fig. 5a. In all cases, we observe a shift of the peaks toward higher temperatures with increasing particle size. This behavior is consistent with an activation energy which rises when size increases (13). In contrast, for the same crystallite size, when the oxygen pressure decreases, especially when the oxygen pressure in the environment during the oxidation is much lower than that in air (14), the maximum oxidation temperature increases (Figs. 5b and 6).

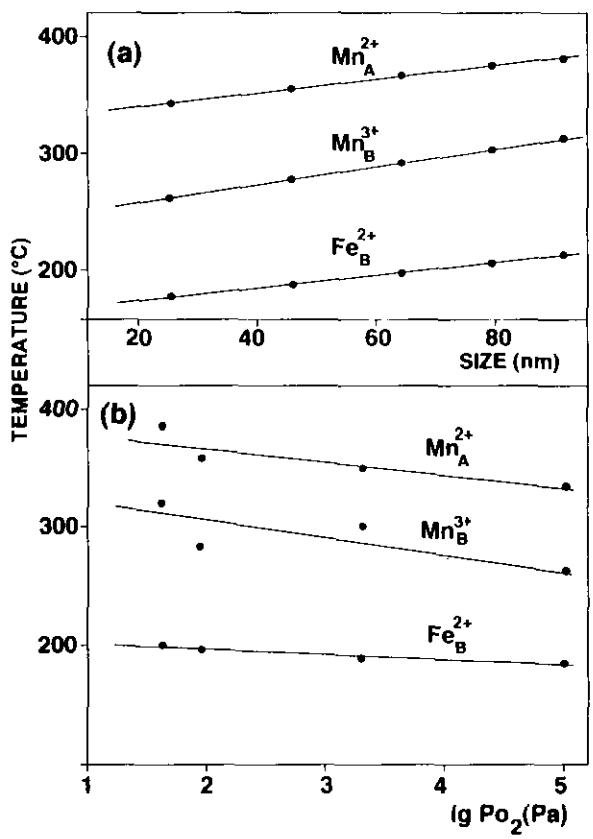

FIG. 5. Effect of (a) crystallite size and (b) oxygen pressure on oxidation peak temperature for $Fe_{3-x}Mn_xO_4$ spinels.

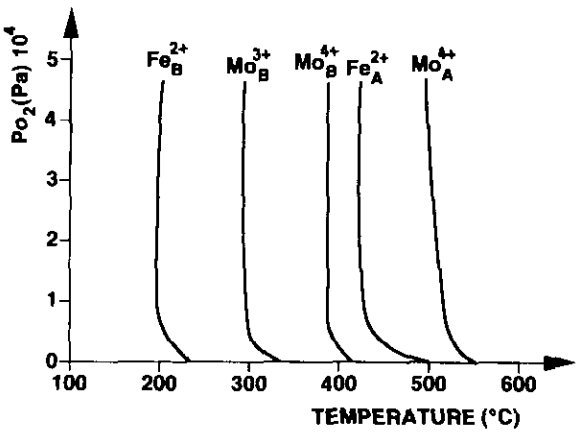

FIG. 6. Effect of oxygen pressure on oxidation temperature peak of iron and molybdenum in $Fe_{3-x}Mo_xO_4$ spinels.

This method can be applied to other divided phases obtained by grinding, and might reveal redox systems such as manganites of transition metals with a spinel (15, 16) or perovskite (17) lattice. For example, the difference in oxidation temperature between copper and nickel manganites pleads in favor of the existence of Cu^+ ions with maintenance of the spinel structure. The DTG curves are compatible with the similar distribution of

$$(Ni^{2+}_{x-\nu}\,Mn^{2+}_{1-x+\nu})_A\,(Ni^{2+}_{\nu}\,Mn^{3+}_{2-2\nu}\,Mn^{4+}_{\nu})_B\,O_4^{2-}$$

and

$$(Mn^{2+}_{1-x}\,Cu^{+}_{x})_A\,(Mn^{3+}_{2-x}\,Mn^{4+}_{x})_B\,O_4^{2-}.$$

That is, in this latter case, there exists an oxidation phenomenon between 230 and 260°C whose amplitude increases with copper content and which corresponds to the oxidation of Cu^+ ions at *A* sites. In these manganites oxidized below 500°C, defect metastable phases could also be brought out subsequent to partial oxidation of the *A*-site Mn^{2+} ions at about 350°C.

DATA TABLE AND CONCLUSION

By characterizing these oxidation mechanisms in submicrometer spinels, we were also able to clearly establish the existence of a correlation between the oxidation temperature and the cation–oxygen bond length for both octahedral and tetrahedral sites of the spinel structure. The oxidation temperature for one cation principally depends on the chemical diffusion coefficient *D* associated at this oxidation (18). Since *D* is a function of the diffusion coefficient of each species, i.e., vacancy, oxidizable cation,

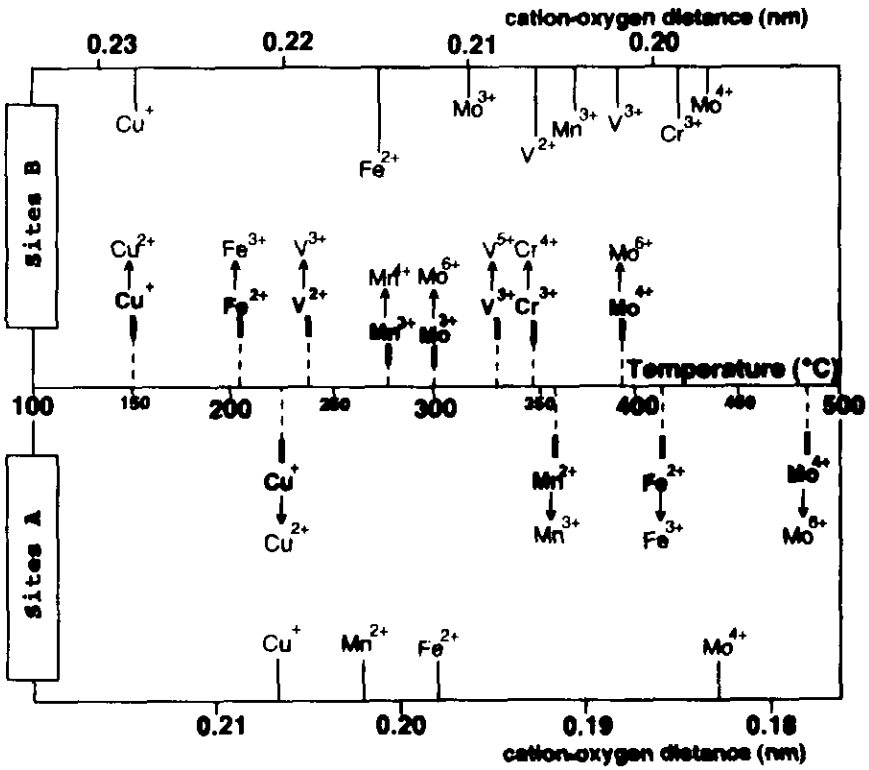

FIG. 7. Data table comparing the oxidation temperatures and the cation–oxygen distances of some oxidizable cations depending on their charge and location in the spinel lattice.

and oxidized cation, it is reasonable to think that the oxidation temperature also depends on the mobility of these three species. Moreover, as the mobility of each species is inversely proportional to different forces which maintain this species in a defined position, it is possible to relate these forces to metal–oxygen distances. The cation–oxygen distances extracted from large numbers of crystal-structure determinations are given by Poix's assumptions (19) concerning the improved bonding rule of Pauling (20) and are reported in Fig. 7 together with the oxidation temperatures. It thus appears that the sequence of oxidation for tetrahedral and octahedral sites is inversely related to the cation–oxygen distance. The greater oxidation temperatures for *A* sites compared to B sites are in accordance with covalent bonds in *A* sites shorter than electrovalent bonds in *B* sites. Hence these simple data are reliable in indicating trends, but not very reliable in giving absolute values, owing to the inevitable distribution in particle sizes and shapes on the one hand and to the relative stretching force constants of the bonds, which depend on numerous factors in the case of transition metals (21), on the other hand. However, within the available precision, the oxidation temperature peak data agree satisfactorily with the inverse of the cation–oxygen distance, as shown in Fig. 7. The cation–oxygen distance of Mo^{3+} ions at *B* sites may be somewhat uncertain since it is very recently that this distance has been established for the first time by Mo *K*-EXAFS (22). A distance of 0.220 nm has been determined, which appeared to be too large when this value was used in the calculation of the lattice constant from the equation developed by Poix (23). The calculated values based on the cationic distribution given in Ref. (12) strongly disagree with the experimental lattice parameters (9). However, we can fit the data very well if we assume a distance of 0.210 nm, which seems more reasonable if we compare this value to other cation–oxygen distances for transition metals in the 3^+ state. Otherwise, if we compare the oxidation temperatures of Mn^{3+} (280°C), Mo^{3+} (300°C), and V^{3+} ions (330°C) with the cation–oxygen distances (0.2045, 0.2100, and 0.2025 nm), it appears that the cation–oxygen distance of the Mo^{3+} ion is again too large and that this distance is between 0.2045 and 0.2025 nm. The disagreement between experimental and predicted values suggests that the cation–oxygen distance may have to be examined more closely. The basic assumption that the cation–oxygen distance increases in the direction V < Mo < Mn can be frustrated by the assignment of formal valence states to the transition metals. Indeed, in the case of $Fe_{3-x}Mo_xO_4$ spinel, Ramdani *et al.* (24) have shown that strong Mo–Mo interactions can be expected within this compound with a modified energy diagram and a nonnegligible covalent contribution to the Mo–O bond.

REFERENCES

1. M. Laarj, I. Pignone, M. El Guendouzi, and B. Gillot, *Thermochim. Acta* **152,** 187 (1989).
2. B. Gillot, F. Chassagneux, and A. Rousset, *Phys. Status Solidi A* **50,** 109 (1978).
3. J. B. Goodenough and A. L. Loeb, *Phys. Rev.* **98,** 391 (1955).
4. B. Gillot and A. Rousset, *J. Solid State Chem.* **65,** 322 (1986).
5. A. Rousset, *Solid State Ionics,* **63–65,** 236 (1993).
6. B. Gillot, B. Domenichini, and A. Rousset, *Ann. Chim. Fr.* **18,** 175 (1993).
7. B. Gillot, M. El Guendouzi, P. Tailhades, and A. Rousset, *React. Solids* **1,** 139 (1986).
8. I. Chassaing, L. Presmanes, P. Tailhades, and A. Rousset, *Solid State Ionics* **58,** 260 (1992).
9. P. Tailhades, L. Bouet, A. Rousset, G. Billot, *C. R. Acad. Sci. Paris Ser. 2* **312,** 1507 (1991).
10. C. Villette, P. Tailhades, and A. Rousset, *C. R. Acad. Sci., Paris Ser. 2* **316,** 1717 (1993).
11. M. Nohair, P. Perriat, B. Domenichini, and B. Gillot, *Thermochim. Acta,* to appear.
12. B. Domenichini, B. Gillot, L. Bouet, P. Tailhades, and A. Rousset, *Solid State Ionics* **58,** 61 (1992).
13. B. Gillot, A. Rousset, and G. Dupre, *J. Solid State Chem.* **25,** 263 (1978).
14. B. Gillot, M. El Guendouzi, *Thermochim. Acta* **162,** 265 (1990).
15. B. Gillot, M. Kharroubi, R. Metz, and A. Rousset, *J. Mater. Chem. Phys.* **26,** 395 (1990).
16. B. Gillot, M. Kharroubi, R. Metz, R. Legros, and A. Rousset, *J. Solid State Chem.* **91,** 375 (1991).
17. A. M. Duprat, P. Alphonse, Ch. Sarda, B. Gillot, and A. Rousset, *J. Mater. Chem. Phys.* **37,** 76 (1993).
18. B. Gillot, *Ann. Chim. Fr.* **3,** 209 (1978).
19. P. Poix, *C. R. Acad. Sci. Paris* **268,** 1139 (1969).
20. L. Pauling, "The Nature of the Chemical Bond," Cornell Univ. Press, Ithaca, New York, 1960.
21. E. Husson and Y. Repelin, *Rev. Chim. Miner.* **22,** 24 (1985).
22. L. Bouet, P. Tailhades, A. Rousset, K. R. Kannan, M. Verelst, G. U. Kulkarni, and C. N. R. Rao, *J. Solid State Chem.* **98,** 123 (1992).
23. P. Poix, *Bull. Soc. Chim. Fr.,* 1985 (1965).
24. A. Ramdani, C. Gleitzer, G. Gavoille, A. K. Cheetman, and J. B. Goodenough, *J. Solid State Chem.* **60,** 269 (1985).